SPECT Using a Specially Designed Cone Beam Collimator

Ronald J. Jaszczak, Kim L. Greer, and R. Edward Coleman

Duke University Medical Center, Durham, North Carolina

A specially designed high resolution converging collimator having a focal length of 50 cm has been evaluated for cone beam single photon emission computed tomography (SPECT). The focal region was investigated by imaging a point source placed at the expected focal point and along the central ray of the collimator in front of and behind the focal point. Technetium-99m point source sensitivities measured in air at 5, 10, 15, and 20 cm from the collimator surface are 4.2, 5.5, 7.3, and 10.5 cts·sec^{-1}·μCi^{-1} when used with a single camera SPECT system. A commercially available parallel hole collimator, with similar resolution characteristics has a measured sensitivity of 3.3 cts·sec^{-1}·μCi^{-1}. Volume sensitivities of 9,780 and 4,945 (cts·sec^{-1})/(μCi·ml^{-1}) were measured for the cone beam and parallel hole collimators, respectively, using a 17-cm-diameter spherical source. Reconstructed spatial resolution (FWHM) on the axis-of-rotation ranged between 10 and 11 mm for both collimators when the radius of rotation was equal to 15 cm. Using equal acquisition times SPECT images of phantoms scanned with the cone beam collimator were visually improved compared with images acquired using the parallel hole collimator. These results demonstrate that a factor of 2 improvement in volume sensitivity can be demonstrated with a cone beam collimator compared with a commercially available parallel hole collimator. Further improvements are possible using shorter focal lengths, astigmatic focusing, and larger field of view cameras.

J Nucl Med 29:1398–1405, 1988

Statistical uncertainties in single photon emission computed tomography (SPECT) can be minimized by the use of a detector system that has a large active area and an acquisition geometry that ensures that as much of the area as possible is being used to detect the emitted gamma photons. Several approaches to improve either single-slice or total-organ sensitivity are being investigated. Systems with banks of closely spaced discrete scanning detectors have been built (*1,2*). A novel system with a geometry consisting of a set of 12 detectors that scan both radially and tangentially has been constructed (*3*). SPECT systems using stationary detector rings coupled with moving collimators are being investigated (*4,5*). At least one system that uses an array of one-dimensional bar cameras has been developed to perform dynamic SPECT acquisitions of xenon-133 in order to estimate regional cerebral blood flow (*6*).

Currently, however, the most widely used SPECT geometry consists of a scintillation camera that rotates about the patient. Camera-based approaches have the advantages of being able to perform both body and brain SPECT imaging as well as conventional planar imaging. SPECT systems using multiple large field-of-view (FOV) scintillation cameras have been built (*7,8*) or proposed (*9*). A high sensitivity annular gamma camera is also being developed for SPECT imaging of the brain (*10*).

To improve further the detection efficiency of a large FOV camera-based SPECT system, several novel collimator geometries are being investigated. These approaches are based on shaping the FOV of the collimator to ensure that the source region of interest is viewed by the largest detector area. For example, collimators having rectangularly shaped holes (*11*) oriented so that the long sides of the rectangles are parallel to the axis-of-rotation, and also sets of axially-focusing collimators (*12*) have been proposed to increase the sensitivity per slice. The former approach degrades axial resolution, while the latter approach results in a set of noncontiguous sections having source regions located between the slices that are not viewed by the camera. However, these tradeoffs may be appropriate for certain imaging situations.

Received Aug. 17, 1987; revision accepted Feb. 23, 1988.

For reprints contact: Ronald J. Jaszczak, PhD, Duke University Medical Center, Dept. of Radiology, Box 3949, Durham, NC 27710.

In imaging the brain using a large FOV camera equipped with a parallel hole collimator, only a small portion of the active detector surface is actually viewing the emitted radiation. As a result of this limitation, Jaszczak et al. (*13*) developed multi-slice fan beam collimators that focuses to a line oriented parallel to the axis-of-rotation. Tsui et al. (*14*) have recently followed this approach in designing a multi-slice fan beam collimator. Fan beam geometry has converging collimation within each slice and parallel collimation along the long axis of the patient. Although this latter characteristic simplifies the reconstruction process (since each slice can be processed separately), detection efficiency is still not optimized since a large portion of the camera is not utilized. To surmount this final limitation, Jaszczak et al. (*15–18*), Hawman et al. (*19*), and Gullberg et al. (*20*) are investigating SPECT geometries that use collimators that converge both transaxially and axially, thereby utilizing nearly all of the active detector area. Previous research efforts by Jaszczak et al. (*15–18*) relating to cone beam SPECT have mainly involved the analysis, simulation, and reconstruction aspects of this type of geometry, although preliminary results obtained using a converging collimator designed for planar imaging have been presented (*21*). This article presents an evaluation of cone beam SPECT (Fig. 1) using a specially designed collimator. The performance of this collimator is compared with a parallel hole collimator having similar resolution characteristics.

METHODS

The cone beam collimator (Nuclear Fields, Inc., Evanston, IL), manufactured using lead casting methodology, has hexagonally shaped holes and a focal length of 50 cm (measured from the front surface of the collimator). A commercially available low-energy, high resolution collimator (Siemens Inc., Des Plaines, IL) (Part Number 810-187A) was used for the parallel beam phantom studies. This collimator is routinely used for most of our clinical and research SPECT scans. The dimensions of the cone beam and parallel hole collimators are presented in Table 1. Projection data for the phantom studies were acquired using one of the gamma cameras of the Duke research SPECT system (*7*).

Technetium-99m (^{99m}Tc) was used for all measurements. A 20% (126–154 keV) energy window was used. For parallel beam acquisitions a secondary energy window (90–124 keV) was used simultaneously with the primary energy window. The projection data contained in the latter window was used to determine the body contour required by the attenuation compensation procedure (*7*). Attenuation compensation for the cone beam data was performed using a recently developed first-order procedure (*18*). Attenuation compensation was used for the phantom images, but not for the patient scan. The attenuating medium was assumed to consist of a cylinder centered on the axis-of-rotation. Flood compensation was performed for both geometries, but scatter compensation was not used. A 15-cm radius-of-rotation was used for both cases.

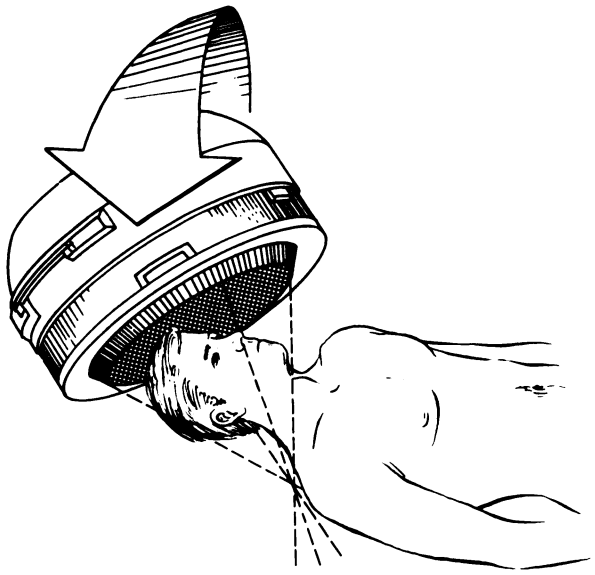

FIGURE 1
Data acquisition geometry for cone beam SPECT.

Planar line source measurements were obtained using a 128 by 128 acquisition matrix.

A filtered backprojection algorithm (*7*) was used for parallel beam data, and a three-dimensional filtered backprojection algorithm based on the approach presented by Feldkamp et al. (*22*) was used for cone beam data. A flow chart of our three-dimensional cone beam algorithm is shown in Figure 2. Linear sampling intervals (within the slice) of 3.2 and 6.4 mm/(pixel-width) were used for parallel beam acquisitions. Along the axis-of-rotation the sampling was typically 6.4 mm/slice for the parallel beam geometry. The finer sampling and 180 angular views (2° frames acquired with continuous gantry rotation) were used to reconstruct images having a matrix size of 128 × 128. The coarser sampling and 90 angular views (4° sampling) were used to reconstruct images having a matrix size of 64 × 64. A generalized Hann (*23*) filter with the parameter f_c (see Reference *23*) equal to four times the Nyquist frequency was used for parallel beam data.

Cone beam data were typically reconstructed into a 64 × 64 × 32 element array. As a result of the magnification characteristics of the cone beam collimator and the reconstruction algorithm, the linear sampling interval was variable and was equal to 4 mm/(pixel-width) at a distance of 15 cm from the collimator surface. Cone beam data were acquired using a 64 × 64 image matrix. For the phantom studies only the central 32 samples were saved in the direction along the axis-of-rotation. For the patient scan 128 axial samples were compressed to 32 samples. Typically, 180 angular frames acquired over 360° with continuous gantry rotation were stored on

TABLE 1
Dimensions of Collimators

Collimator	Hole shape	Focal length f (cm)	Collimator thickness a (cm)	Hole size d (cm)	Septal thickness t (cm)
Parallel hole	Square	—	2.46	0.115	0.015
Cone beam	Hexagonal	50	4.06	0.190	0.025

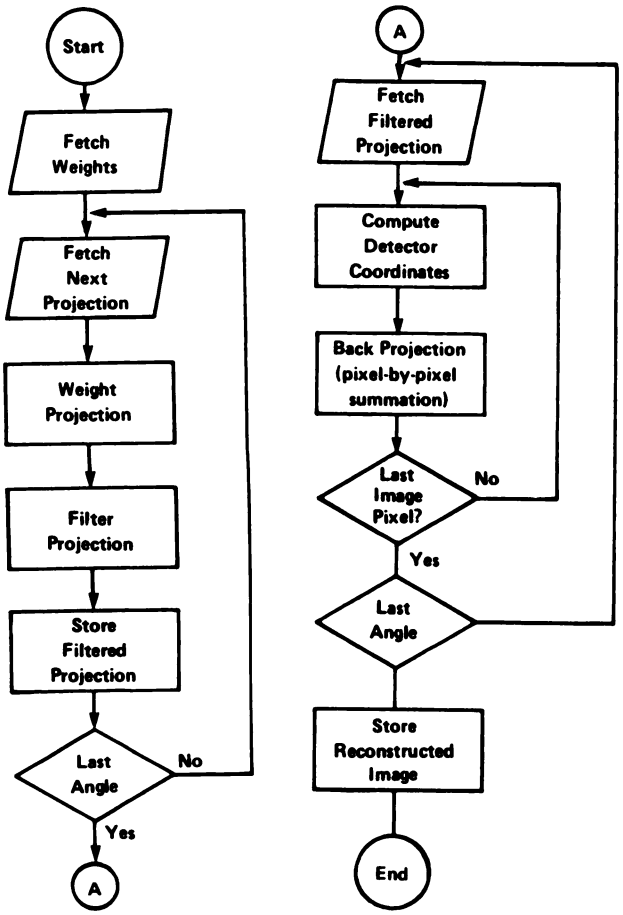

FIGURE 2
Flow diagram of three-dimensional cone beam reconstruction algorithm.

magnetic tape for later image reconstruction. For the cone beam data, a ramp filter or a generalized Hann filter with the parameter f_c (see Reference *23*) equal to 5 cycles/cm was used. The frequency responses of the filters used for the parallel hole and cone beam geometries are very similar and resulted in equivalent resolutions (FWHM) as measured using line sources. As suggested by Feldkamp et al. (*22*), the projection data were not filtered in the direction along the axis-of-rotation. The phantom data and line source measurements were acquired with the collimator surface oriented parallel to the axis-of-rotation. For display purposes the cone beam images were reduced to the same size as the parallel beam images. Furthermore, to obtain nearly equivalent slice thicknesses (for the cone beam and parallel hole geometries) three transaxially formatted cone beam sections were added together resulting in an overall slice thickness of 12 mm. These images were then compared with the sum of two slices (thickness equal to 12.9 mm) obtained with the parallel hole collimator.

The focal region of the cone beam collimator was investigated by obtaining planar images of a point source located at the expected focal point, and at positions in front of and behind the focal point. The sheet source response of the parallel hole and cone beam collimator was qualitatively evaluated using a large, water-filled disk containing a uniform distribution of ^{99m}Tc. Glass capillary tubes (inside diameter ~ = 1 mm) filled with ^{99m}Tc were used to measure the planar and the in-plane SPECT spatial resolutions [full width at half maximum (FWHM) and full width at tenth maximum (FWTM)]. The field-of-view (FOV) of the cone beam collimator was estimated by moving a point source (~ 2 mm in diameter) parallel to the face of the collimator at six distances from the collimator surface. The FOV was defined as a circle whose diameter was determined by locating points in space where the counting rate fell to 50% of its maximum value. A point source, measured in air, was used to determine the sensitivity. The volume sensitivity was determined using a water-filled spherical source (17 cm in diameter) containing a uniform concentration of ^{99m}Tc. The center of the spherical source was placed at a distance of 15 cm from the collimator surface. To qualitatively evaluate lesion detectability, a 3-cm-diameter photon deficient sphere was placed within a commercially available cylindrical phantom (Data Spectrum Corp., Chapel Hill, NC) (18 cm inside diameter) containing a uniform distribution of ^{99m}Tc and scanned for equal time intervals using both collimators. Low-count density (100,000 counts per slice for the parallel hole geometry) transaxial sections were then evaluated, both visually and by plotting profiles through the region containing the photon-deficient sphere. For the patient study, 14 mCi of ^{99m}Tc-labeled methylenediphosphonate (MDP) was injected intravenously 1 hr prior to scanning the head for 18 min using a clinical SPECT system (ZLC 7500, Siemens Gammasonics, Inc). The camera was tilted at an angle of 19° from the axis-of-rotation to optimize the useful field-of-view. The reconstruction algorithm was appropriately modified to account for the tilted acquisition. The parallel beam patient scan was acquired with a commercially available high resolution collimator (Siemens) (Part Number 825-00654) have hexagonally shaped holes. A ramp filter was used for the cone beam and parallel hole scans.

The parallel hole collimator and SPECT gantry used for the patient study were not the ones that were used for the phantom studies. Although the two parallel hole collimators have different hole shapes, both collimators (and SPECT systems) have similar resolution and sensitivity characteristics. The main differences relate to the physical shape of the housing and method of mounting. The patient collimator was not available for the phantom investigations. A special adaptor was obtained which allowed the cone beam collimator to be mounted on both systems. The use of the clinical SPECT camera was required for the cone beam patient scan since it has the capability to acquire tilted angle projection data.

RESULTS

Point and Sheet Source Results

Images of a point source located on the central ray of the cone beam collimator and placed at the nominal focal point (50 cm), and at 5 cm in front of and behind the focal point are shown in Figure 3. These images contain ~ 5 million detected events. Although some residual collimator hole misalignments are indicated by these images, the overall quality was judged to be markedly superior to similar scans we have previously obtained (*21*) using a converging collimator designed for planar imaging.

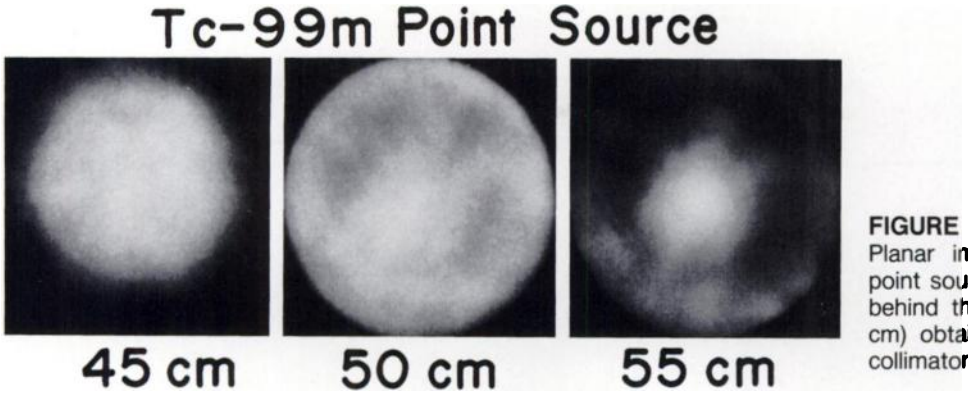

FIGURE 3
Planar images of a ^{99m}Tc-labeled point source located in front of and behind the nominal focal point (50 cm) obtained with the cone beam collimator.

A sheet source image (Fig. 4) obtained with the cone beam collimator is similar to the corresponding image obtained with the parallel hole collimator. The profiles drawn through the parallel hole and cone beam images are nearly identical. The residual similar features seen in both profiles most likely relate to the intrinsic response of the gamma camera and analog-to-digital converter. Sheet source images similar to the ones shown in Figure 4, except with increased count densities, may be used to compensate for regional sensitivity variations (i.e., flood compensation) for both parallel hole and cone beam geometries. However, residual collimator hole angulation errors would require a different compensation for both collimator geometries.

The field-of-view of the cone beam collimator was measured as described in the methods section. These results are presented in Table 2. As a result of the sensitivity change with angular displacement, these measurements only estimate the collimator's useful field-of-view. Furthermore, tilting the camera also changes the useful imaging volume.

Collimator Sensitivities

A comparison of the measured (in air) point source sensitivities for the cone beam and high resolution parallel hole collimators are presented in Figure 5. At a distance of 15 cm, the point source sensitivity for the cone beam collimator is more than twice that of the parallel hole collimator. For the cone beam results, the source was located along the central ray of the collimator.

The change in sensitivity as a function of angular displacement from the central ray of the cone beam collimator was evaluated by moving a source within a plane located at a distance of 15 cm from the collimator surface. This plane was parallel to the collimator surface. These results are shown in Figure 6.

Volume sensitivities for both collimator geometries were measured using the 17-cm-diameter spherical source. With the center of the source placed at a distance of 15 cm from the collimator surface, the volume sensitivity of the cone beam collimator is equal to 9,780 $(cts \cdot sec^{-1})/(\mu Ci \cdot ml^{-1})$. This value is approximately twice as large as the volume sensitivity of the parallel hole collimator, which is equal to 4945 $(cts \cdot sec^{-1})/(\mu Ci \cdot ml^{-1})$.

Spatial Resolution

A comparison of the measured system spatial resolutions (full width at half maximum for planar imaging) for both collimator configurations is shown in Figure 7. The results include the effect of the camera's intrinsic resolution which is 5.1 mm (FWHM). The spatial resolution of the cone beam collimator is nearly identical

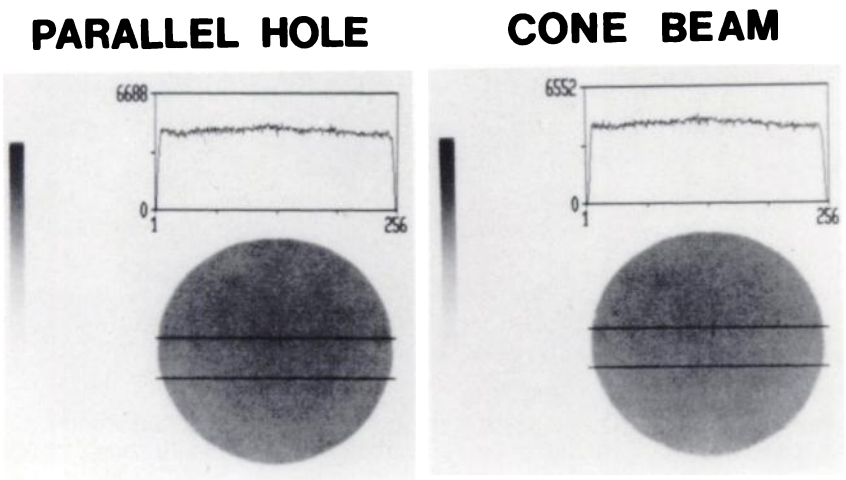

FIGURE 4
Images (5 million counts) with profiles of a ^{99m}Tc-labeled sheet source obtained with a parallel hole (left) and cone beam (right) collimators.

TABLE 2
Field-of-View of Cone Beam Collimator

Distance to collimator surface (cm)	Diameter of field-of-view (cm)
0	36
5	32
10	28
15	24
20	20
25	16

to the spatial resolution of the high resolution parallel hole collimator for distances between 5 and 25 cm from the collimator surface. The cone beam measurements were made along the central ray of the collimator. We also evaluated several off-axis locations (at a fixed distance from the collimator surface) and observed no large changes in planar spatial resolution.

The reconstructed spatial resolution for the cone beam collimator (measured at the intersection of the axis-of-rotation and the central ray of the collimator) was 10.6 mm (FWHM) when the radius-of-rotation was 15 cm. The reconstructed spatial resolution (measured on the axis-of-rotation) for the parallel hole collimator was 11.0 mm when the radius-of-rotation was 15 cm. The reconstructed resolution for the cone beam collimator degraded by approximately one to two millimeters when the radius-of-rotation was increased to 20 cm.

Phantom and Patient Scans

Reconstructed images of a 3-cm-diameter photon deficient sphere within a water-filled cylinder (18 cm diameter) containing a uniform distribution of ^{99m}Tc are shown in Figure 8. The sphere was positioned ~ 2 cm from the central axis of the cylinder. The projection data for both geometries were acquired for equal scan durations. The parallel hole geometry contained ~ 100,000 counts per slice. A low-count density was selected for this study so that the noise level would be large. Profiles through the images of the phantom at a level containing the sphere are shown at the bottom of the figure. The cone beam profile indicates decreased noise as compared with the parallel hole profiles, and the lesion is most easily visualized in the cone beam scan. For the parallel hole geometry, both 128 × 128 and 64 × 64 reconstruction matrices have been presented. The Nyquist frequency for the cone beam reconstruction is equal to 1.25 cycles/cm, while the Ny-

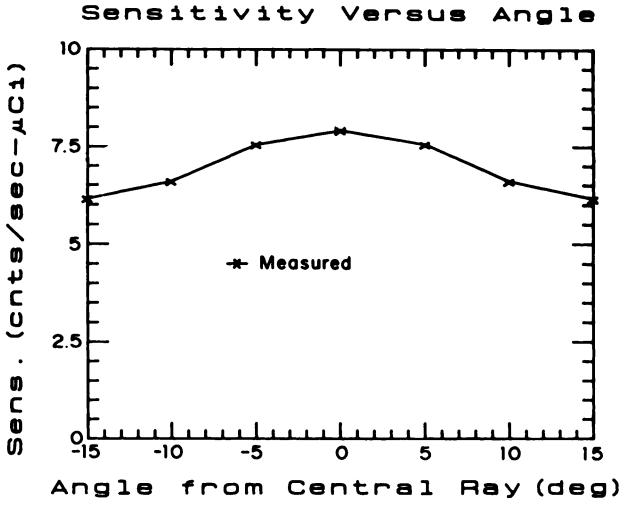

FIGURE 6
The change in point source sensitivity of the cone beam collimator as a function of angular displacement from the central ray measured at a distance of 15 cm from the collimator surface.

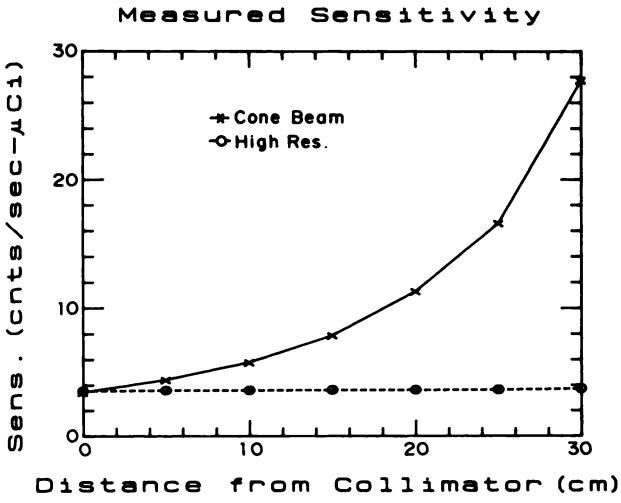

FIGURE 5
Sensitivities of the cone beam and high resolution parallel hole collimators measured in air using a ^{99m}Tc-labeled point source.

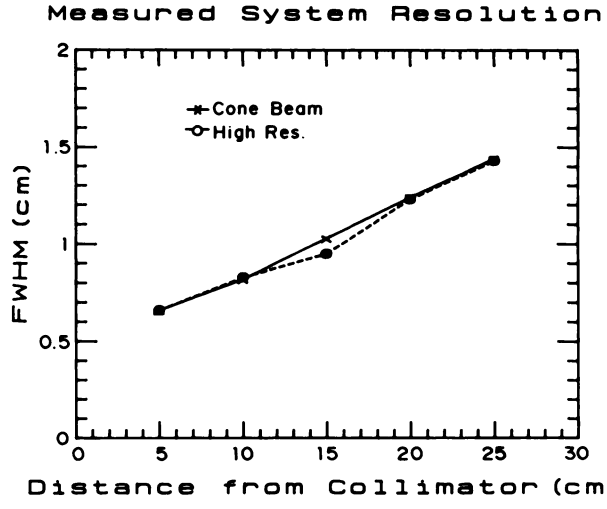

FIGURE 7
Spatial resolutions (planar) for the cone beam and high resolution parallel hole collimators measured using a ^{99m}Tc-labeled line source.

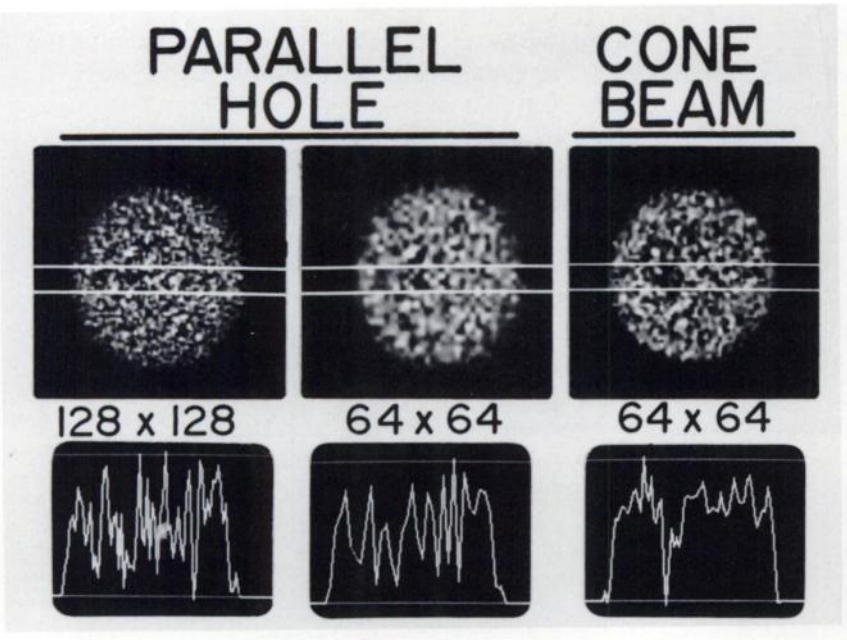

FIGURE 8
Low count density SPECT images (acquired for equal scan times) of a 3-cm photon deficient sphere positioned within a cylinder containing uniform activity.

quist frequencies for the 128 × 128 and 64 × 64 parallel hole reconstructions are equal to 1.57 and 0.79 cycles/cm, respectively. Thus, the cutoff frequency used for the cone beam filter has a value that is between the two values used for the parallel hole geometry. Following reconstruction, the cone beam images were minified to equal the size of the parallel hole images. The pixel-slice thickness are nearly the same for all reconstructions.

Cone beam images of the patient scan are shown in Figure 9. For the cone beam acquisition, the patient's head was re-positioned to approximately correspond to its position during the parallel hole acquisition. A slight distortion in count densities can be seen in the most superior region of the skull on the sagittal section. Attenuation compensation was not used for the patient scans. For the parallel hole scan, a total of, ~ 34,000 counts per slice were acquired for each transaxial section. Because of cone beam magnification, pixel dimensions for the parallel hole and cone beam images shown in Figure 9 are similar, but not exactly identical.

DISCUSSION

A specially designed and built cone beam collimator has been evaluated and compared with a parallel hole collimator. For equivalent spatial resolution the cone beam collimator offers the potential for a gain in volume sensitivity of a factor of 2 as compared with a commercially available parallel hole collimator. The results obtained with the photon-deficient sphere, acquired with equal acquisition times, indicate that cone beam SPECT may lead to improved lesion detectability.

Careful quality control procedures must be used during collimator manufacture and prior to data acquisition. If the individual collimator holes are not all aimed toward a common focal point, the SPECT image may be degraded. Using a converging collimator designed for planar imaging, we have previously (*21*) observed that a spatial resolution degradation of 2 mm (FWHM) in the reconstructed image as compared with the planar scan. This converging collimator had an astigmatic focal region. Planar images of a point source placed near the nominal focal point resulted in two orthogonal bands of intensity. The cast collimator used in the

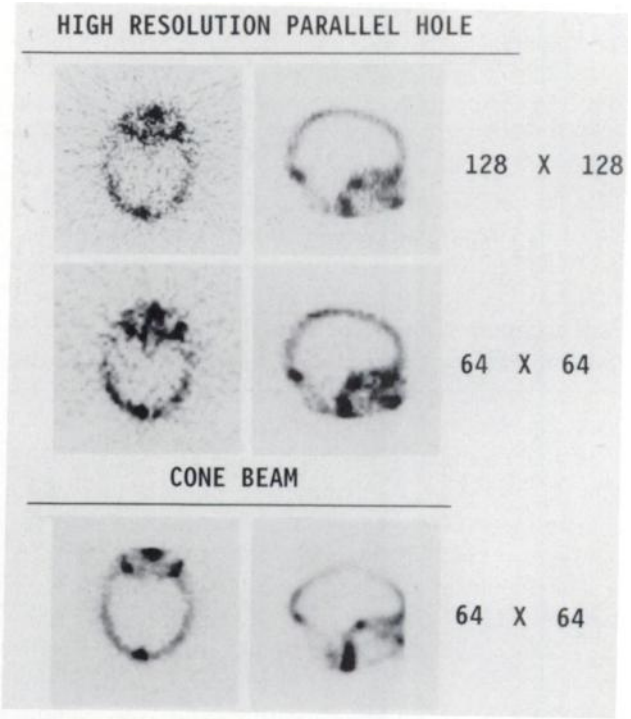

FIGURE 9
Parallel hole (top) and cone beam (bottom) SPECT images of a patient scanned with equal acquisition times.

present study did not exhibit this type of astigmatic focusing (see Fig. 3). Manufacturing accuracy is thus important for cone beam SPECT, although it may be possible to develop software corrections to compensate for systemic errors.

As with parallel hole collimators, flood compensation is required with cone beam collimation to remove residual sensitivity variations. We have evaluated our present software by taping a U.S. coin ($.25) on the collimator surface to introduce a known, localized nonuniformly. A water-filled sphere (17 cm diam.) containing a uniform distribution of ^{99m}Tc was scanned with the cone beam collimator. An 82 million count planar image of a ^{99m}Tc sheet source was used to generate flood correction factors. Reconstructed SPECT images (not presented here) with and without flood compensation were compared. The compensation algorithm essentially eliminated the gross circular artifact introduced by the coin that was taped to the collimator. Because of the three-dimensional nature of the geometry, the propagation of errors resulting from sensitivity variations will be different than the errors for parallel geometry. We have found that our software functions work well for parallel hole collimation and equally well for cone beam collimation.

Center-of-rotation calibration is also required for cone beam SPECT. In the present study, this calibration was performed manually by placing a point source on the axis-of-rotation and computing its centroid. Recently, a curve-fitting procedure has been proposed for determining the parameters of a cone beam collimator (*20*). Of course, a routine quality control protocol, such as imaging a standard test phantom, would still be required for cone beam SPECT. It is not anticipated that the magnitude of the problems associated with quality control for cone beam geometry should be markedly different than the problems associated with parallel hole collimation. Although the mathematical equations describing cone beam geometry may appear more complicated as compared with parallel hole geometries, many of the aspects relating to quality control have a common physical origin. It should be noted, for example, that a parallel hole collimator may be described as a cone beam collimator having a very long focal length.

A slight artifact was observed in the patient scan. This type of event-mispositioning was not observed in the scans of phantoms, which were acquired with the camera parallel to the axis-of-rotation.

The distortion may be the result of incomplete sampling and the lack of appropriate filtering along the axis-of-rotation. The backprojection algorithm proposed by Feldkemp et al. (*22*) results in transverse sections that are all identical for axially symmetrical objects; however, for a more generalized source distribution, an axial blurring, or mispositioning of detected events, will occur. When the collimator surface is parallel to the axis-of-rotation, this distortion is absent for the midplane slice that contains the central ray of the cone beam collimator. As the cone angle increases (i.e., moving away from the slice containing the central ray), the magnitude of the distortion increases. Longer focal length collimators result in reduced distortion as compared with shorter focal length collimators.

A focal length of 50 cm was selected to ensure an adequate field-of-view for imaging the brain. For the patient scan, it was necessary to tilt the camera with respect to the axis-of-rotation to minimize the separation between the collimator and the skull activity and to optimize the circular field-of-view of the camera so that the projections would not be truncated. This tilting effectively increases the maximum cone angle for rays that are viewing the superior portion of the skull, thereby increasing distortion at those locations.

We are investigating iterative reconstruction approaches and modifications to the filter as possible solutions for eliminating, or at least minimizing, this distortion. Other groups (*19*) are investigating the use of a displacement in the central ray of the collimator to reduce the maximum cone angle. Further work is also required in developing efficient methods for determining the body contour and implementing an appropriate procedure for attenuation compensation. When these aspects have been successfully addressed, cone beam collimation should result in improved SPECT imaging of the brain. Furthermore, if distortions associated with truncated projections can be minimized (perhaps by using iterative algorithms), cone beam SPECT may result in even greater improvements in imaging other small organs such as the heart.

ACKNOWLEDGMENTS

The authors thank Wendy Painter for her excellent secretarial support.

This investigation was supported by PHS Grant No. CA33541, awarded by the National Cancer Institute.

REFERENCES

1. Kuhl DE, Edwards RQ, Ricci AR, Yacob RJ, Mich TJ, Alavi A. The Mark IV system for radionuclide computed tomography of the brain. *Radiology* 1976; 121:405–413.
2. Cho ZH, Yi W, Jung KJ, Lee BU, Min HB. Performance of single photon tomographic system-Gammatom-1. *IEEE Trans Nucl Sci* 1982; NS-29:484–487.
3. Moore SC, Doherty MD, Zimmerman RE, Holman BL. Improved performance from modifications to the multidetector SPECT brain scanner. *J Nucl Med* 1984; 25:668–691.
4. Rogers WL, Clinthorne NH, Stamos J, et al. Performance evaluation of SPRINT, a single photon ring tomograph for brain imaging. *J Nucl Med* 1984; 25:1013–1018.

5. Hirose Y, Ikeda Y, Higashi Y, Koga K, Hattori H. A hybrid emission CT-HEADTOME II. *IEEE Trans Nucl Sci* 1982; NS-29:520–523.
6. Stokely EM, Sveinsdottir E, Lassen NA, Rommer P. A single photon dynamic computer assisted tomography (DCAT) for imaging brain function in multiple cross-sections. *J Comput Assist Tomogr* 1980; 4:230–240.
7. Jaszczak RJ, Chang LT, Stein NA, Moore FE. Whole-body single-photon emission computed tomography using dual, large-field-of-view scintillation cameras. *Phys Med Biol* 1979; 24:1123–1143.
8. Lim C, Gottschalk S, Schreiner R, et al. Triangular SPECT system for brain and body organ 3-D imaging: design concept and preliminary imaging results [Abstract] *J Nucl Med* 1984; 25:P6.
9. Budinger TF. Physical attributes of single-photon tomography. *J Nucl Med* 1980; 21:579–592.
10. Logan KW, Holmes RA. Missouri University multiplane imager (MUMPI): a high sensitivity rapid dynamic ECT brain imager [Abstract] *J Nucl Med* 1985; 25:P105.
11. Jaszczak RJ. Collimator trans-axial tomographic scintillation camera. United States Patent Number 4,057,726, 1977.
12. Lim CB, Chang LT, Jaszczak RJ. Performance analysis of three camera configurations for single photon emission computed tomography. *IEEE Trans Nucl Sci* 1980; NS-27:559–568.
13. Jaszczak RJ, Chang LT, Murphy PH. Single photon emission computed tomography using multi-slice fan beam collimators. *IEEE Trans Nucl Sci* 1979; NS-26:610–618.
14. Tsui BMW, Gullberg GT, Edgerton ER, et al. The design and clinical utilities of a fan beam collimator for a SPECT system [Abstract]. *J Nucl Med* 1985; 25:P5.
15. Jaszczak RJ, Floyd CE, Manglos SH, Greer KL, Coleman RE. Cone beam collimation for SPECT: Analysis, simulation and image reconstruction using filtered backprojection. *Med Phys* 1986; 13:484–489.
16. Jaszczak RJ, Floyd CE, Manglos SH, Greer KL, Coleman RE. Three-dimensional single-photon emission computed tomography using cone beam collimation (CB-SPECT). In: *Engineering of computerized multi-dimensional imaging and processing (1986).* SPIE Vol. 671. Washington: The Society of Photo-optical Instrumentation Engineers, 1986 193–199.
17. Floyd CE, Jaszczak RJ, Greer KL, Coleman RE. Cone beam collimation for SPECT: simulation and reconstruction. *IEEE Trans Nucl Sci* 1986; NS-33:511–514.
18. Manglos SH, Floyd CE, Jaszczak RJ, Greer KL, Coleman RE. A practical attenuation compensation method for cone-beam reconstruction. *IEEE Trans Nucl Sci* 1987; NS-34:294–298.
19. Hawman EG, Hsieh J. An astigmatic collimator for high sensitivity SPECT of the brain [Abstract]. *J Nucl Med* 1986; 27:930.
20. Gullberg GT, Tsui BMW, Crawford CR. A method for estimating the parameters of a cone beam detector for SPECT [Abstract]. *J Nucl Med* 1987; 28:661.
21. Jaszczak RJ, Floyd CE, Manglos SH, Greer KL, Coleman RE. Cone-beam SPECT: Experimental validation using a conventionally-designed converging collimator [Abstract]. *J Nucl Med* 1986; 27:930.
22. Feldkamp LA, Davis LC, Kress JW. Practical cone-beam algorithms. *J Opt Soc Am* 1984; 1:612–619.
23. Jaszczak RJ, Coleman RE, Whitehead FR. Physical factors affecting quantitative measurements using camera-based single photon emission computed tomography (SPECT). *IEEE Trans Nucl Sci* 1981; NS-28:69–80.